Interferometric Measurements of Re-Entry Vehicle Base Radius

R. L. Henry*
U.S. Air Force Systems Command, Wright-Patterson Air Force Base, Ohio

The expected accuracy of a proposed technique to measure the base radius of re-entry vehicles at ranges of several hundred kilometers is described. It is shown that a plausible aircraft-mounted intensity interferometer should be capable of measuring the base radius of a nominal 20 cm base radius, 14,000 kg/m^2 ballistic coefficient re-entry vehicle to an uncertainty of 0.96 cm at a range of 277.5 km. This figure includes the degrading effects of photon shot noise, the turbulence and attenuation in the atmosphere between the aircraft and the re-entry vehicle, and the uncertainty in the atmospheric structure constant. The corresponding expected base radius uncertainty for measurements on a nominal 35 cm base radius, 8500 kg/m^2 ballistic coefficient re-entry vehicle is 0.68 cm. The aircraft carrying the interferometer is assumed to be flying above the tropopause, which lies at an altitude below 10.67 km at latitudes far from the equator in the winter. This paper includes a brief theoretical description of the effects of atmospheric turbulence on the output of an intensity interferometer.

Nomenclature

a = temperature correlation length of boundary-layer turbulence
A_d = area of detector
A_{rv} = projected area of re-entry vehicle
B = bandwidth of a detector and its associated electronics
c = vacuum speed of light
C_D = drag coefficient
$C_e(L)$ = correlation from interferometer with extended detector observing an extended source
C_n^2 = atmospheric index of refraction structure constant
$C_{PA}, C_{P'A}$ = amplitudes of electric field at point A of light from points P and P', respectively
C_W = empirical constant related to temperature differences across a turbulent boundary layer
D_Φ = variance of phase difference between two points
E_A = electric fields of light at point A
E_i = exponential integral
f = difference between the local and average index of refraction of air
f_i = integration variable
$F_A(\omega-\omega')$ = response function of detector and electronics at point A to signals modulated at $(\omega-\omega')$
h = variable for integration over altitude
h_1, h_2 = altitudes of aircraft and source, respectively
H = air density scale height
I_A = intensity of radiation at point A
L = center-to-center separation of detectors
L_b = thickness of turbulent aircraft boundary layer
M_∞ = Mach number of refraction of freestream air
n_0 = number of photons per unit area per unit optical frequency at the detectors at wavelength of peak detector sensitivity
$n(\omega)$ = spectrally dependent number of photons per unit area per unit optical frequency
N = index of refraction of air
$P_r(x,y)$ = radiance emitted from point (x,y) on the source surface
Q = phase
r = base diameter of re-entry vehicle
r_N = nose radius of re-entry vehicle
r_w = radius of wake a distance x_w downstream of the re-entry vehicle
$R^2(\Delta p_f)$ = sum of square of residuals resulting from the change of a parameter by Δp_f
R_0 = nominal distance from target to instrument
$R_{PA}, R_{P'A}$ = optical path lengths to point A from point P and P', respectively
s = separation of points P and P'
s_{s+}, s_{s-} = atmospheric turbulence scale distances associated with $\Delta\psi_+$ and $\Delta\psi_-$, respectively
S_A = output of amplifier A
$\langle S_A S_{A'} \rangle_A$ = correlation in the presence of atmospheric turbulence
S/N = ratio of interferometer signal to photon shot noise
t = time
T = air temperature
T_{ave} = time period for averaging
T_e = exposure time
T_W = air temperature at surface of aircraft fuselage
u_∞ = aircraft airspeed
x, x', y, y' = integration variables
X, X', Y, Y' = integration variables
x_w = distance downstream from the re-entry vehicle
y_n = distance of instrument from aircraft nose
v_e = magnitude of initial re-entry vehicle velocity
$V(\omega_0)$ = viewing factor for the average optical frequency ω_0, which includes the atmospheric transmission, the R_0^2 reduction in irradiance due to distance, and other such effects
α = angular width of source
$\alpha_e(X,Y)$ = quantum efficiency of point (X,Y) on the detector
α_0 = average quantum efficiency in the narrow optical region where the detectors are sensitive
$\alpha(\omega)$ = spectrally dependent detector quantum efficiency
β = ballistic coefficient
$\Delta(\omega_0)\Gamma^2(L,\omega_0)$ = correlation factor

Received Feb. 8, 1988; revision received July 30, 1988. This paper is declared a work of the U.S. Government and is not subject to copyright protection in the United States.

*Aerospace Engineer, Foreign Technology Division. Senior Member AIAA.

γ = ratio of specific heat at constant pressure and volume of air
γ_e = initial re-entry angle
δ_{PA} = variation in optical path length from point P to point A due to atmospheric turbulence
ϵ_i = instrument efficiency factor
η = normalized spectral density of detector amplifier combination
θ,θ' = angles between normal to line AA' and lines from center of AA' to points P and P'
θ_c = cone angle of sphere cone of re-entry vehicle
θ_0 = average of θ and θ', the nominal direction of source
ν_∞ = kinematic viscosity of freestream air
ρ = air density
σ = variance of temperature
σ_n^2 = variance of photon shot noise
$\sigma_{(N-1)}^2$ = variance of difference from unity of index of refraction of air
σ_{rc}^2 = variance of apparent width correction
σ_{rp}^2 = variance of re-entry vehicle radius due to photon shot noise
σ_R^2 = variance of optical path length R
$\sigma_{ss\pm}^2$ = uncertainty in the atmospheric scale distance $ss\pm$
$\sigma_{(1/T)}^2$ = variance of reciprocal of temperature
σ_d = normalized spectral density of light at detectors
$\Phi_{AP}, \Phi_{AP'}$ = phases of electric field at point A from points P and P', respectively
$X_p, X_{p'}$ = initial phases of light emitted from points P and P', respectively
ψ_+,ψ_- = sum and difference of phases of electric fields at P and P'
$\Delta\psi$ = change in ψ_- due to presence of atmospheric turbulence
$\Delta\psi_+,\Delta\psi_-$ = components of $\Delta\psi$ proportional to sum and difference of ω and ω', respectively
$(\Delta\psi_-)_a, (\Delta\psi_-)_b$ = components of $\Delta\psi_-$ due to paths outside of and inside the aircraft boundary layer, respectively
$\Psi(L,p_f)$ = normalized interferometer output for detector separation L and parameter value p_f
ω,ω' = frequency of radiation from points P and P', respectively
$\langle\ \rangle$ = time average
$|\ |$ = absolute value

Subscripts (if not otherwise defined)

A,A' = locations of detectors
d = detector
e = experimental signals
max = maximum value
P,P' = locations of sources
t = theoretical signals

Introduction

THE expected accuracy of a proposed technique to measure the base radius of re-entry vehicles (RV) at ranges of several hundred kilometers is described. The proposed technique utilizes an intensity interferometer of the Hanbury Brown-Twiss type[1-6] mounted on an aircraft flying above the tropopause. A knowledge of basic vehicle dimensions such as base radius is essential for the understanding of the aerodynamic characteristics of any aerodynamic vehicle, including a RV. The base radius of a RV is of particular interest because it has a significant effect on the RV aerodynamic drag and hence the RV contribution to the overall accuracy of the missile system. Since vehicle dimensions are normally readily available to the missile system analyst, there has been little interest in developing techniques to measure them. Cases do exist where measurement techniques are needed because of some uncertainty in the vehicle dimensions prior to re-entry. Reference 7 describes a wideband radar measurement technique that is applicable to a wide class of vehicle measurements, including measurements of RV base radius. This paper examines the proposed application of intensity interferometry, an astronomical technique originally developed to measure the diameter of stellar radio sources, to the measurement of RV base radius. Since this technique utilizes the infrared self-emissions of the body during the latter stages of re-entry, the potential for high-resolution measurements is improved over that of radar measurements due to the relatively shorter wavelength of the infrared radiation. In addition, since the proposed measurements are to be made during the latter stage of re-entry, this technique is particularly applicable to measurements of changes that occur during the earlier re-entry stages.

This paper shows that with some viewing scenarios and with current technology, it is theoretically feasible to measure the base radius of a nominal 0.2 m base radius, 14,000 kg/m^2 ballistic coefficient RV to an uncertainty of 0.0021 m (1.0%) at a range of 277.5 km with an intensity interferometer of plausible specifications. The corresponding expected uncertainty for measurements on a nominal 0.35 m base radius, 8500 kg/m^2 ballistic coefficient RV is 0.0055 m (1.6%). These estimates include the degrading effects of photon shot noise, the attenuation of the optical emissions by the atmospheric absorption, the degrading effects of the turbulence in the aircraft boundary layer and the remainder of the atmosphere between the aircraft and the RV, and the uncertainty in the knowledge of the atmospheric structure constant. They assume that the aircraft carrying the interferometer is flying above the tropopause, which lies at an altitude below 10.67 km at latitudes far from the equator in the winter. The paper is organized as follows: a theory describing the influence of atmospheric turbulence on intensity interferometry measurements is developed, a plausible intensity interferometer suitable for aircraft mounting is described, the expected viewing scenario and RV characteristics is provided, the expected measurement uncertainty is calculated, and the effects of RV wake are briefly discussed.

Influence of Atmospheric Turbulence

An interferometer to the Hanbury Brown-Twiss type operates by measuring the correlations in the time of arrival of the naturally occurring fluctuations in the light from a source at physically separated detectors. These correlations are dependent on the separations and on the angular width of the source as viewed from the instrument. Since photons obey Bose-Einstein statistics,[8] the photons in a beam of light are bunched together. From the standpoint of classical physics, this bunching can be represented by beat frequencies between optical waves of slightly different frequencies that modulate the resulting beam intensity.[1] This modulation can be detected with high-speed detectors. If only a single detector is used, it is not possible to distinguish this modulation from noise. If two detectors are used to observe the same source, the noise in the outputs from each detector is uncorrelated, while the modulation in the optical beam is present in the output of each detector. Therefore, the high-frequency outputs from each detector are correlated. This correlation is a function of the separation of the detectors, the bandwidth of the detectors and their associated electronics, and the angular width of the source.[1,2] Intensity interferometry has been discussed extensively in the literature. In particular, the signal-to-photon-shot-noise ratio, extended source effects, and other details have been exhaustively discussed.[2-6]

The influence of the atmosphere between an intensity interferometer and a RV is dependent upon the angular width of the RV, the instrument bandwidth, and the properties of the intervening atmosphere. An understanding of the important parameters relevant to this discussion can be made by examin-

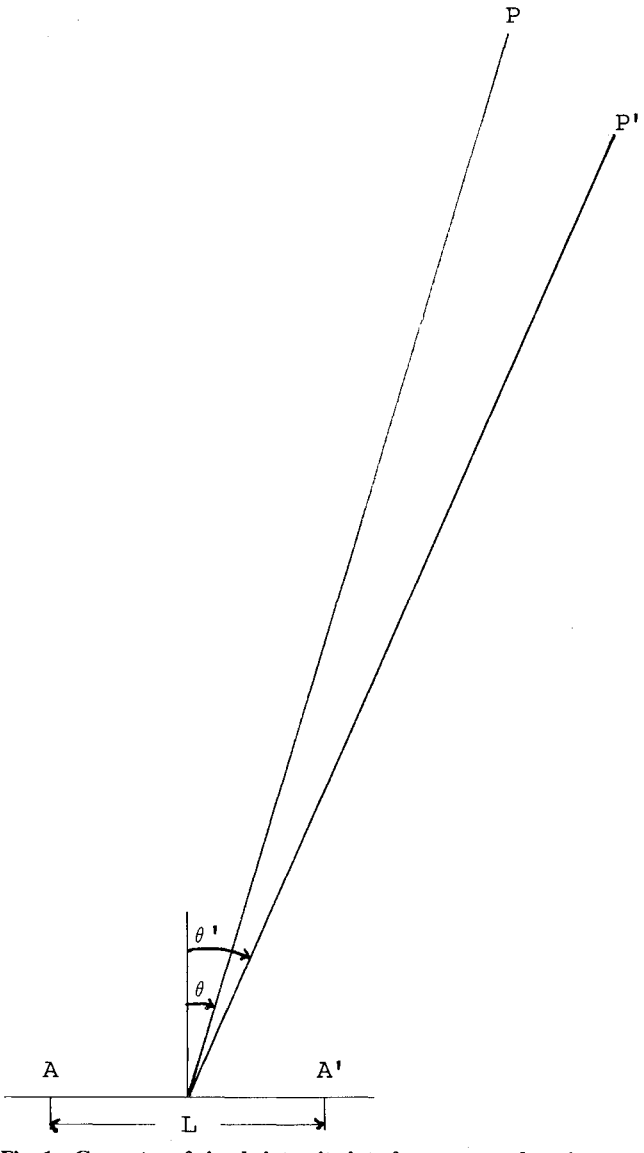

Fig. 1 Geometry of simple intensity interferometer used to view two objects, of angular width $\theta - \theta'$, at points P and P' (detectors at points A and A' are separated by length L).

ing the simplest possible intensity interferometer scenario capable of yielding a source angular width measurement. Consider the following geometry. Two detectors at points A and A' observe a target consisting of two point sources at P and P' that emit light at angular frequencies ω and ω', respectively. (See Fig. 1.) Let the nominal distance R_0 between the sources and the detectors be much greater than the detector separation L and the source separation s. Therefore, the light incident upon a detector from a source is a good approximation to a plane wave. Let the angles between the perpendicular to the line joining the detectors and the lines from either detector to the points P and P' be θ and θ', respectively. The electric field at point A due to the sources at point P and P' is

$$E_A = C_{PA} \cos(\Phi_{AP}) + C_{P'A} \cos(\Phi_{AP'}) \tag{1}$$

For the purposes of this discussion, C_{PA} and $C_{P'A}$ can both be taken to the unity,

$$\Phi_{AP} = \omega t - R_{PA}(\omega/c) - \mathrm{X}_P \tag{2}$$

and

$$\Phi_{AP'} = \omega' t - R_{P'A}(\omega'/c) - \mathrm{X}_{P'} \tag{3}$$

The phases X_P and $\mathrm{X}_{P'}$ are assumed to be random variables.[9] The expressions for the waves at point A' can be obtained from Eqs. (1-3) by replacing A with A'. The irradiance at point A is proportional to E_A^2. Hence,

$$I_A = \propto 2[1 + \cos(\Phi_{AP} - \Phi_{AP'})] \cos^2[(\Phi_{AP} + \Phi_{AP'})/2] \tag{4}$$

If the detector is connected to an amplifier that does not pass direct current, the amplifier output S_A is the product of the frequency response function of the amplifier and its associated electronics and the coefficient of $\cos^2\{[(\omega + \omega')/2]t + Q\}$ in Eq. (4),

$$S_A = V^{1/2}(\omega_0) F_A(\omega - \omega') \cos(\Phi_{AP} - \Phi_{AP'}) \tag{5}$$

Similarly,

$$S_{A'} = V^{1/2}(\omega_0) F_{A'}(\omega - \omega') \cos(\Phi_{A'P} - \Phi_{A'P'}) \tag{6}$$

For simplicity, assume the coefficients F_A and $F_{A'}$ are identical. The correlation in the outputs of the two amplifiers is given by the time average of their product $\langle S_A S_{A'} \rangle$,

$$\langle S_A S_{A'} \rangle = V(\omega_0) \langle \tfrac{1}{2}[F_A(\omega - \omega')]^2 [\cos(\psi_+) + \cos(\psi_-)] \rangle \tag{7}$$

$$\psi_+ = \Phi_{AP} - \Phi_{AP'} + \Phi_{A'P} - \Phi_{A'P'} \tag{8}$$

$$= 2(\omega - \omega')t - (1/c)[\omega(R_{PA} + R_{PA'}) - \omega'(R_{P'A} - R_{P'A'})] - (X_P - X_{P'}) \tag{9}$$

and

$$\psi_- = \Phi_{AP} - \Phi_{AP'} - \Phi_{A'P} + \Phi_{A'P'} \tag{10}$$

$$= -(1/c)[\omega(R_{PA} - R_{PA'}) - \omega'(\mathrm{R}_{P'A} - R_{P'A'})] \tag{11}$$

Because of the presence of the random phases X_P and $\mathrm{X}_{P'}$, the time average of $\cos(\psi_+)$ vanishes. Since the field at the detectors from each source is approximately a plane wave,

$$R_{\mathrm{PA}} - R_{PA'} = L \sin(\theta) \tag{12}$$

and

$$R_{P'A} - R_{P'A'} = L \sin(\theta') \tag{13}$$

Combining the above expressions and noting the α is small,

$$\langle S_A S_{A'} \rangle = \tfrac{1}{2} V(\omega_0)[F_A(\omega - \omega')]^2 \times \cos\{(L/c)[(\omega - \omega') \sin(\theta_0) + \alpha(\omega + \omega') \cos(\theta_0)/2]\} \tag{14}$$

The above expression illustrates the existence of a relationship between the correlation of the signal from two detectors, the angular width of the target, and the interferometer baseline. The more detailed analysis in Ref. 3 obtains the correlation when the detectors view an extended target and provides an expression from the signal-to-photon-shot-noise ratio S/N.

The atmosphere degrades the correlation by introducing random differences in the path lengths. These arise because temperature variations caused by turbulence induce index of refraction variations in both the boundary layer and the free-stream air surrounding the aircraft carrying the instrument. A realistic instrument uses detectors with nonzero width collecting areas and temporal bandwidths to measure targets with nonzero width areas. The correlation expression obtained from a detailed analysis of such an instrument is identical to Eq. (7)—aside from containing integrals over detector areas, bandwidths, and optical sensitivities and containing integrals over source areas. Therefore, the degradation of the interferometer output by the turbulent atmosphere can be understood by examining the correlation expression given in Eq. (7).

Denote the uncertainty in the length of a portion of the optical path by a δ with the same subscripts as those of that portion. For example, the uncertainty in the optical path from a source at point P to a detector at point A is denoted δ_{PA}. These add the quantity $\Delta\psi$ to ψ_- given in Eq. (11), as

$$\Delta\psi = -(1/c)[\omega(\delta_{PA} - \delta_{PA'}) - \omega'(\delta_{P'A} - \delta_{P'A'})] \quad (15)$$

$$= \Delta\psi_+ + \Delta\psi_- \quad (16)$$

where

$$\Delta\psi_+ = [(\omega + \omega')/2c][(\delta_{PA} - \delta_{P'A}) + (\delta_{P'A'} - \delta_{PA'})] \quad (17)$$

and

$$\Delta\psi_- = \frac{(\omega - \omega')}{c}\left[\frac{(\delta_{PA} - \delta_{PA'}) + (\delta_{P'A} - \delta_{P'A'})}{2}\right] \quad (18)$$

There are two characteristic length scales for the path length uncertainty that has been illustrated. The scale length for the quantity $\Delta\psi_+$, which is proportional to the sum of the path length uncertainties for paths from different points on the target to the same detector, is the average of the optical wavelengths represented by ω and ω'. This scale length determines the size of the source region in which intensity interferometer measurements are possible. In contrast, the scale length for the quantity $\Delta\psi_-$, which is proportional to the average of the differences in the path length uncertainties for paths from each point on the target to the two different points on the detectors, is the effective wavelength represented by the frequency difference divided by the speed of light. This latter scale length determines the ultimate resolution of the intensity interferometer measurements.

The correlation in the presence of these path length uncertainties, $\langle S_A S_{A'}\rangle_A$, is

$$\langle S_A S_{A'}\rangle_A = \tfrac{1}{2} V(\omega_0)[F_A(\omega - \omega')]^2 [\cos(\psi_-)\langle\cos(\Delta\psi)\rangle - \sin(\psi_-)\langle\sin(\Delta\psi_+)\rangle] \quad (19)$$

Equation (19) shows that path length uncertainties effect the correlation in two ways: 1) they cause the addition of a second term, proportional to $\sin(\psi_-)$, whose detector spacing dependence is 90 deg out of phase with that of the unmodified correlation and 2) they cause the term proportional to the original unmodified correlation to be reduced by a factor of $\langle\cos(\Delta\psi)\rangle$. Consider the former effect first. The additional term is proportional to $\langle\sin(\Delta\psi)\rangle$. The argument of the sine function has equal probability of being positive or negative. Since the sine is an odd function, it also has equal probability of being either positive or negative. Therefore, the average value of $\sin(\Delta\psi)$ vanishes.

Now consider the term proportional to $\langle\cos(\Delta\psi)\rangle$. If $\Delta\psi$ is a random variable with a normal distribution, it is easily shown that

$$\langle\cos(\Delta\psi)\rangle = \exp[-\langle(\Delta\psi)^2\rangle/2] \quad (20)$$

Using Eq. (16), the argument of this term can be written as the sum of two quantities, $\Delta\psi_+$ and $\Delta\psi_-$. The first quantity is a function of the angular width of the source, as viewed from the detector. For narrow sources, the light from different points transverses the same atmospheric inhomogeneities. Therefore, the atmospheric path length uncertainties for light from different target points to the same detector are the same and $\Delta\psi_+$ vanishes. For wide sources, the light from different points transverses different atmospheric inhomogeneities, the atmospheric path length uncertainties for light from different target points to the same detector are different, and $\Delta\psi_+$ is nonzero.

For the portion of the optical path through the aircraft boundary layer, the optical paths from various points on a RV viewed at a range of several hundred kilometers are sufficiently close together that they transverse the same inhomogeneities. Hence, these portions of the optical paths do not contribute to $\Delta\psi_+$. The portion of the optical paths from the RV to the outside of the aircraft boundary layer requires more careful examination. Since light rays are reversible, these path length uncertainties are the same as those that would be experienced if the light was emitted from the detector and traveled to the source. The details of this latter process have been extensively studied in the literature.[10-12] The variance of the phase difference between two points on the resulting wavefront separated by a distance s is

$$D_{\Phi+} = 2.91\left(\frac{\omega}{c}\right)^2 \frac{R_0}{(h_2 - h_1)} \int_{h_1}^{h_2} C_n^2(h)\left[\frac{(h - h_1)s}{(h_2 - h_1)}\right]^{5/3} dh \quad (21)$$

In this expression, we have accounted for the convergence of the light rays from the two points on the source to a single point on the detector, neglected Earth curvature and atmospheric refraction, and assumed that both the phase difference and index of refraction uncertainties have zero means. For notational simplicity and to allow for possible future atmospheric data inputs, it is convenient to define a scale distance s_{s+}, which corresponds to the source point spacing[12] where $D_{\phi+}$ is equal to 6.88. Hence, s_{s+} is defined such that path length variations for light from points that are angularly separated by less than the s_{s+} are correlated, as

$$s_{s+} = 3.18\left\{2.91\left(\frac{\omega}{c}\right)^2 \frac{R_0}{(h_1 - h_2)} \times \int_{h_1}^{h_2} C_n^2(h)\left[\frac{(h - h_1)}{(h_1 - h_2)}\right]^{5/3} dh\right\}^{-3/5} \quad (22)$$

This expression accounts for the reduction in the spacing between the rays as the light travels from each source to a detector. The average of the optical path length uncertainties from different points on the target to one detector are equal to those to the other detector. Therefore,

$$\langle(\Delta\psi_+)^2\rangle = 13.76(s/s_{s+})^{5/3} \quad (23)$$

Now consider the quantity $\Delta\psi_-$. Since they are the result of independent random processes, the variance of the optical path length uncertainty difference is the sum of the variances from the portions of the paths inside and the portions outside the boundary layer. The optical path length uncertainties for those portions of the optical paths outside the aircraft boundary layer can be obtained with an expression very similar to Eq. (21). This new expression differs from Eq. (21) in that it uses the difference of the optical frequencies of the two sources, equal to the bandwidth of the detectors and their associated electronics, rather than their average and, in that, it accounts for the divergence of the light rays in their paths to the two separate detectors. The variance of the phase difference between two points separated by a distance X on a wavefront from a point on the source $D_{\Phi-}$, is

$$D_{\Phi-} = 2.91\left(\frac{\omega - \omega'}{c}\right)^2 \frac{R_0}{(h_2 - h_1)} \int_{h_1}^{h_2} C_n^2(h)\left[\frac{X(h_2 - h)}{(h_2 - h_1)}\right]^{5/3} dh \quad (24)$$

Hence, the contribution to $\Delta\psi_-$ from those portions of the optical path outside of the aircraft boundary layer $(\Delta\psi_-)_a$ is given by

$$\langle(\Delta\psi_-)_a^2\rangle = 6.88(X/s_{s-})^{5/3} \quad (25)$$

where the scale distance s_{s-} is given by

$$s_{s-} = 3.18\left\{2.91\left(\frac{\omega-\omega'}{c}\right)^2 \frac{R_0}{(h_2-h_1)} \times \int_{h_1}^{h_2} C_n^2(h)\left[\frac{(h_2-h)}{(h_2-h_1)}\right]^{5/3} \mathrm{d}h\right\}^{-3/5} \tag{26}$$

Because of the high aircraft airspeed, the optical path length changes induced by the boundary layer in front of each detector are independent random processes. The optical path itself is equal to the integral of the average atmospheric refraction over the path between the target and the detector. The variance of this average σ_R^2 can be obtained using an argument by Bramley,[13]

$$\sigma_R^2 = \frac{L_b^2}{T_{\text{ave}}}\int_0^{T_{\text{ave}}}\left(\frac{1}{L_b}\int_0^{L_b} f(x,t)\,\mathrm{d}x - \frac{1}{T_{\text{ave}}L_b}\int_0^{L_b}\int_0^{T_{\text{ave}}} f(x,t')\,\mathrm{d}t'\,\mathrm{d}x\right)^2 \mathrm{d}t \tag{27}$$

The function $f(x,t)$ can be written as the product of a time-varying random variable $h(t)$ and a spatially varying random variable $g(x)$. Assume that the autocorrelation function of $g(x)$ is given by $\exp(-x^2/a^2)$, where a is the spatial correlation length.[14] Then,

$$\sigma_R^2 = L_b^2\sigma_{N-1}^2\int_0^1 (1-u)\exp\left\{\frac{-x^2u^2L_b^2}{a^2}\right\}\mathrm{d}u \tag{28}$$

Using the Gladstone-Dale expression[15] and the ideal-gas law,

$$\sigma_{N-1}^2 = (N-1)_\infty^2\sigma_{(1/T)}^2 \tag{29}$$

$$\sigma_R^2 = (N-1)_\infty^2\frac{\sigma_{T^2}}{T_\infty^2}aL_b\sqrt{\pi} \tag{30}$$

Since the radii of curvature of the fuselage of an aircraft is much larger than the thickness of the aircraft boundary layer, this boundary-layer thickness can be approximated by that of a turbulent boundary layer over a flat plate,[15] as

$$L_b = 0.37y_n(u_\infty y_n/\nu_\infty)^{-1/5} \tag{31}$$

The spatial correlation length a is typically one-tenth of the boundary-layer thickness. The temperature differences inside the boundary layer will be approximated by the difference between the temperature of the aircraft wall and that of the freestream air as[16]

$$T_W/T_\infty = 1 + \tfrac{1}{2}C_W(\gamma-1)M_\infty^2 \tag{32}$$

where C_W is an empirical constant equal to 0.85 for laminar and 0.88 for turbulent boundary layers, respectively. The contribution of the boundary layer to $\langle(\Delta\psi_-)^2\rangle$, $\langle(\Delta\psi_-)_b^2\rangle$ is given by

$$\langle(\Delta\psi_-)_b^2\rangle = \frac{2(\omega-\omega')^2}{c^2}(N-1)_\infty^2\left(\frac{T_W}{T_\infty}\right)^2\frac{aL_b}{\sqrt{\pi}} \tag{33}$$

while correlations between $\Delta\psi_-$ and $\Delta\psi_+$ undoubtedly exist, the large difference between the scale lengths appropriate to each quantity means that little error is introduced if these values are combined by adding their variances.

A nonzero value for $\Delta\psi$ has two effects: it reduces the correlation obtained from a finite-width source and it changes the apparent source width. The former effect reduces the signal-to-noise ratio and, hence, reduces the accuracy of the apparent source width. While it is possible to correct for the latter systematic effect, uncertainties in the correction factor reduce the accuracy of the final result. Aside from the atmospheric effects, the dominant noise source is photon shot noise resulting from the quantum nature of light. This noise is similar to the well known shot noise in electronic circuits.[17] The overall uncertainty in the base radius measurement σ_r is the sum of the uncertainty resulting from photon shot noise σ_{rp} and the uncertainty resulting from the apparent width correction σ_{rc}.

The width of a source is obtained from intensity interferometer data by fitting the experimental data to a theoretical model using the source width as a fitting parameter. To eliminate errors caused by the source intensity variations, uncertainty in the atmospheric transmission, and instrument drift, it is customary to normalize the data collected from physically separated detectors with the signal obtained by two detectors that view the source through the same path by means of a beam splitter. In the presence of a normally distributed noise source with variance σ_n^2, the variance of a single parameter obtained with this procedure, in this case σ_{rp}^2, is given by

$$\sigma_{rp}^2 = \frac{(\Delta r)^2}{R^2(\Delta r)(M-1)} \tag{34}$$

where

$$R^2(\Delta p_f) = \sum\frac{\{\Psi[L,(p_f+\Delta p_f)]_t - \Psi(L,p_f)_e\}^2}{\sigma_n^2} \tag{35}$$

where the sum runs the M pairs of physically separated detectors.[18]

The reduction in correlation by the atmosphere of the signal from the outer edges of a source causes the source to appear smaller than its actual width. If this width change is small, the uncertainty in the correction σ_{rc}^2 is

$$\sigma^2 rc = \frac{-R^2(\Delta s_+)\sigma_{ss+}^2}{(\Delta s_+)^2} - \frac{R^2(\Delta s_-)\sigma_{ss-}^2}{(\Delta s_-)^2}\Big/\frac{R^2(\Delta r)}{(\Delta r)^2} \tag{36}$$

To apply the preceding statistical expressions, it is necessary to compute only the theoretical instrument output-to-photon-shot-noise ratio S/N, rather than the actual theoretical instrument output itself. When the region of optical sensitivity of the detectors is narrow and the detector/amplifier combinations are identical, Ref. 3 shows that this is given by

$$S/N = \epsilon_i\beta_0A_d\{BT_e\}^{1/2}\eta^{-1/2}\alpha_0n_0\sigma d\Delta(\omega_0)\Gamma^2(L,\omega_0) \tag{37}$$

where ϵ_i is dependent upon such quantities as the loss of correlation in the optical and electronic equipment, the noise produced by the detector amplifier combination, the excess noise in the electronic equipment, and stray light. The polarization factor is given by

$$\beta_0 = 2[n_{0\perp}^2 + n_{0=}^2]/n_0^2 \tag{38}$$

where the subscripts $\perp$ and $=$ refer to the two orthogonal directions of polarization. In addition,

$$B = \frac{\int_0^\infty |F(f_i)|^2\,\mathrm{d}f_i}{F_{\max}^2} \tag{39}$$

$$\eta = \frac{\int_0^\infty |F^4(f_i)|\,\mathrm{d}f_i}{F_{\max}^2\int_0^\infty |F(f_i)|^2\,\mathrm{d}f_i} \tag{40}$$

$$\sigma_d = \frac{\int_0^\infty \alpha^2(\omega)n^2(\omega)\,\mathrm{d}\omega}{\alpha(\omega_0)n(\omega_0)\int_0^\infty \alpha(\omega)n(\omega)\,\mathrm{d}\omega} \tag{41}$$

By comparing Eqs. (7) and (19) with Eq. (A11) of Ref. 3, the generalization of the correlation factor, $\Delta(\omega_0)\Gamma^2(L,\omega_0)$, to include the effects of atmospheric turbulence is given by

$$\Delta(\omega_0)\Gamma^2(L,\omega_0) = \int\int\int\int\int\int\int\int_{A_d A_d' A_{rv} A_{rv}'} P_r(x,y)\, P_r(x',y') \times \alpha_e(X,Y)\alpha_e(X',Y')$$

$$\times \exp\left\{-6.88\left[\frac{(x-x')^2+(y-y')^2}{s_{s+}^2}\right]^{5/6}\right\} \times \exp\left\{-3.44\left[\frac{(X-X')^2+(Y-Y')^2}{s_{s-}^2}\right]^{5/6}\left(\frac{B}{\omega_0}\right)^2\right.$$

$$\left.-\frac{B^2}{c^2}(N-1)_\infty^2\frac{T_W^2}{T_\infty^2}aL_b\sqrt{\pi}\right\} \times \cos\left[\frac{\omega_0}{c}\frac{(x-x')}{R_0}(X+L-X')\right] dX\, dY\, dX'\, dY'\, dx\, dy\, dx'\, dy' \qquad (42)$$

where x and x' are coordinates on the source parallel to the detector separation, y and y' are coordinates on the source perpendicular to the detector separation, X and X' are coordinates on the detectors parallel to the detector separation, Y and Y' are coordinates on the detectors perpendicular to the detector separation, the integrals are over the projected areas of the source and detectors, and the possibility that the detector sensitivity may be nonuniform is included in the detector quantum efficiencies. Using conventional error propagation relations, the signal-to-noise ratio of the normalized signal is $\sqrt{2}$ times that given in the preceding expression.

Since the atmospheric turbulence viewing characteristics change with target altitude, it is necessary to integrate the target altitude dependent square of the photon shot noise limited resolution per exposure time over the altitude region corresponding to the exposure period. The time difference Δt necessary for the RV to travel from altitude h_i to h_f is given by[19]

$$\Delta t = \left(\frac{H}{v_e \sin\gamma_e}\right)\left\{E_i\left[\frac{H\rho(h_f)}{2\beta\sin\gamma_e}\right] - E_i\left[\frac{H\rho(h_i)}{2\beta\sin\gamma_e}\right]\right\} \qquad (43)$$

The overall apparent width correction will be computed by averaging over the exposure interval with $R^2(\Delta r)$ as the weighting function.

Instrument Specifications

To estimate the accuracy of a measurement technique for a particular application, it is necessary to specify some instrument parameters. While the following description appears plausible, it has not been adjusted for optimum performance and is not intended to constitute a final instrument design. An interferometer consisting of a linear arrangement of square telescopes provides more collecting area and more sensitivity than a similar interferometer consisting of the same number of round telescopes occupying the same physical volume. This occurs because squares nest more closely than circles and, hence, use the available space more efficiently. The interferometer will be assumed to consist of a linear array of five 21.5 cm square reflecting telescopes spaced with their centers 25 cm apart, see Fig. 2. This size square objective can be cut from readily available 30.48 cm round mirrors. This telescope separation provides a maximum center-to-center telescope separation of 1 m and still provides 3.4 cm between adjacent telescopes for objective mounting and alignment. The reduction in collecting area due to the possible presence of a secondary mirror of a Cassegrain or Newtonian optical arrangement will be ignored, since the reduction on instrument sensitivity caused by the obscured area is small and since the exact reduction is intimately dependent upon telescope design. An optical arrangement similar to an off-axis parabolic telescope would eliminate the secondary mirror at the expense of increased telescope cost. The largest practical number of telescopes will not provide enough samples of the theoretical interference pattern to distinguish between multiple objects. Hence, it will be necessary to restrict the telescope fields of view so that only one object is visible at a given time. This, plus the angular motion of the RV during re-entry, will require that the instrument track the intended target during the collection.

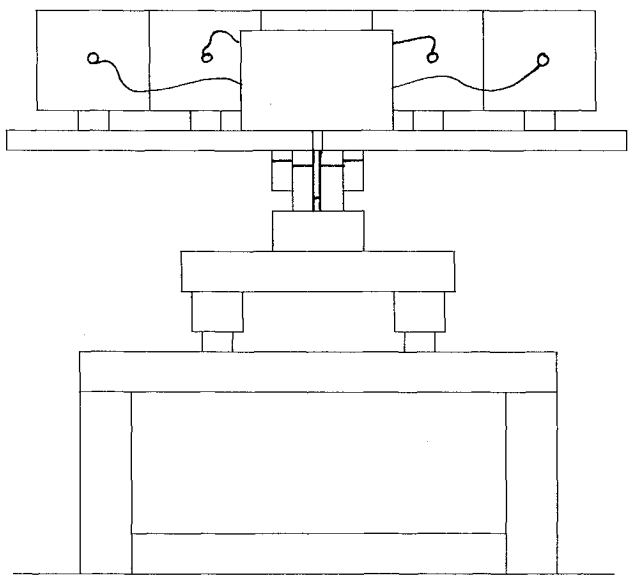

Fig. 2 Back view of proposed aircraft mounted intensity interferometer.

An optimum detector will have a peak spectral sensitivity that is both close to the peak of the spectral distributions of the radiation emitted during the ablation of common heat shield materials (roughly 1 μm for silica phenolic and 0.7 μm for carbon) and at as long a wavelength as possible to minimize the atmospheric turbulence effects described in Eqs. (21) and (24). In addition, the operating bandwidth of the optimum detector and its associated electronics will be as large as possible to maximize the signal-to-photon-shot-noise ratio discussed earlier. We will assume that the detectors are sensitive in a narrow optical band centered about 1.5 μm, have a quantum efficiency of 0.475, and have an electronic bandwidth of 1 GHz. These values appear reasonable since a detector with double this quantum efficiency and 10 times this electronic bandwidth was described in a paper published in 1975.[20] The detector in this reference did have its peak sensitivity at a somewhat shorter value, 1.06 μm.

The remaining instrument parameters will be conservatively taken to be those of the original 1950's era intensity interferometer described in Ref. 3. In particular, σ_d will be taken as 0.451 and η will be taken as 0.98. The Ref. 3 value of $\beta_0 = 0.96$ appears plausible because of the expected atmospheric transmission of 0.95. The remaining instrument characteristics will be assumed to yield a value for ϵ_i of 0.81.

Viewing Scenario and Re-Entry Vehicle Description

This instrument will be assumed to be mounted in an aircraft flying at an altitude of 10.67 km. The atmospheric conditions will be taken to be those described by the 60° north latitude January atmosphere of the 1966 U.S. Standard Atmosphere.[21] At latitudes far from the equator in the winter, this aircraft

altitude is above the tropopause. Using the sea level value for the visible light index of refraction of air, 1.0002926, and the Gladstone-Dale expression, the index at the aircraft altitude is 1.00008339. The structure constant altitude profile will be taken to be that given by Hufnagel's night model.[22] Since the tropopause associated spike in this structure constant profile appears at an altitude higher than 10.67 km and since we have assumed that the tropopause lies below this altitude, Hufnagel's profile will be adjusted by assuming that the structure constant decreases with increased altitude from its value immediately below the spike in Hufnagel's profile. The altitude dependence will be taken to be that observed above the spike in Hufnagel's profile. Therefore, the structure constant along the viewing path will be taken to be

$$C_n^2 = 3.78 \times 10^{-17} h^{-5/2} \text{cm}^{-2/3} \text{km}^{5/2} \quad (44)$$

This yields results that are consistent with direct measurements of the structure constant.[23]

The expected accuracy of the values of s_{s+} and s_{s-} is also necessary to estimate the measurement accuracy. At sea level, direct measurements show that the values of s_{s+} and s_{s-} vary by about 20%.[24] To analyze field data, it will be necessary to compute s_{s+} and s_{s-} from a theoretical altitude profile of C_n computed from a theoretical model of such quantities as the rate of energy per unit mass dissipated by viscous friction and the average shear rate of the wind. The former quantity depends on such parameters as the air density and viscosity. The accuracy of the computed values of s_{s+} and s_{s-} are dependent upon the source of the information. The presence of the aircraft carrying the intensity interferometer provides an opportunity to obtain atmospheric information that will establish boundary conditions that the theoretical atmosphere model must meet. For example, comparison of pressure altitude with altitude from a radar altimeter provides a measure of the atmospheric pressure at the aircraft altitude. Measurements of the temperature profile of the atmosphere outside the aircraft as it climbs to cruising altitude will both definitely show if the aircraft has passed through the tropopause into the stratosphere (the air temperature increases with increasing altitude in the stratosphere and decreases with increasing altitude in the troposphere) and will yield the air density outside the aircraft when combined with the radar and pressure altitude values. In addition, the aircrew will have some knowledge of the direction and speed of the winds, at the aircraft altitude, from which the average wind shear rate can be estimated. An alternative method for measuring s_{s+} might be developed from the attenuation in correlation that occurs when an attempt is made to image targets that have dimensions exceeding s_{s+}. Since RV optical wakes are many tens of meters long, intensity interferometric measurements along the RV wake should yield equivalent widths related to s_{s+}. (Please note that RV optical wake length is a function of both the bandpass of the viewing system and the definition used to determine when the wake radiation level has declined to a negligible level.) We will assume that s_{s+} and s_{s-} will both be known to an uncertainty of 20%, the same variation as that in the sea level measurements.

A transport-type aircraft will be assumed because aircraft of this type are capable of carrying an instrument package above the tropopause. The aircraft airspeed will be taken to be 280 m/s, corresponding to an aircraft Mach number of 0.91. This is high (and therefore conservative) for an aircraft of this type. The instrument will be assumed to be mounted 10.67 m aft of the aircraft nose. This mounting position and the operating bandwidth of 1 GHz discussed earlier result in a value for $\langle(\Delta\psi_-)_b^2\rangle$ of 2.97×10^{-7}. The above structure-constant profile and viewing scenario result in a value for s_{s-} in excess of 82 km at the lowest, most affected target altitude considered here. Therefore, $\Delta\psi_-$ has a negligible effect on the instrument output.

Detailed modeling of the spatial intensity profile of a RV and its wake is far beyond the intended scope of this paper. Simple models of two different RV's, representing medium and high ballistic coefficient vehicles, will be considered. For comparison, both vehicles will be assumed to be spherically blunted 7.5 deg cones with 5 cm nose radii and silica phenolic heat shields re-entering at a nominal 24 deg re-entry angle with initial re-entry velocities of 6 km/s. For the purpose of relating elapsed time to vehicle altitude, an average atmospheric density scale height of 6.7 km will be assumed. Both vehicles will be assumed to be foreshortened by viewing at a 45 deg angle between the cone axes of symmetry and the instrument line of sight. They will be assumed to be oriented such that the axes of symmetry are perpendicular to the line joining the interferometer detectors. The lower performance vehicle will be taken to be a 0.7 m base diam, 7500 kg/m^2 ballistic coefficient vehicle with surface roughness properties that cause laminar-to-turbulent boundary-layer transition to occur at an altitude such that the entire vehicle surface is at the peak silica phenolic ablation temperature of 2700 K over the altitude region extending from roughly 25 to 12 km. The comparable range for an otherwise identical higher performance 0.4 m base diameter, 14,000 kg/m^2 ballistic coefficient vehicle will be taken to be 18 to 13 km. Since the heat shield is assumed to be uniform in temperature in these regions, they are also expected to radiate as Lambertian surfaces of uniform radiance.

Expected Measurement Accuracy

The altitude dependence of the elapsed time from the start of the data collection, the atmospheric scale distance associated with the average optical frequency, the expected photon shot noise limited base radius uncertainty per square root exposure time, and the expected error in the apparent width correction due to uncertainty in the atmospheric scale distance for the vehicles, the instrument, and the viewing scenario described above are listed in Table 1.

For the higher-performance vehicle, the expected photon shot noise limited base radius uncertainty, obtained by integrating over the entire altitude range, is 0.134 cm. The rms average of the expected error resulting from the apparent width correction, weighted by the reciprocal of the photon shot noise per square root exposure time uncertainty, is 0.073 cm. This yields an overall expected base radius uncertainty of 0.206 cm. The corresponding values for the medium performance vehicle are 0.058 cm for the expected photon shot noise limited base radius uncertainty obtained by integrating over the entire altitude range, 0.493 cm for the expected rms average of the error due to the apparent width correction weighted by the reciprocal of the photon shot noise per square root exposure time uncertainty, and 0.551 cm for the expected overall base radius uncertainty.

Wake Effects

While detailed modeling of the spatial intensity profile of a RV wake is far beyond the intended scope of this paper, it is

Table 1 Expected photon limited resolution and apparent width error

RV altitude, km	s_s+, cm	Elapsed time, s	Photon noise limited radius resolution per square root time, cm · s$^{-1/2}$	Apparent width error, cm
		Medium-performance vehicle		
25.00	188.0	0.00	0.112	0.248
21.75	160.2	1.40	0.129	0.326
18.50	133.2	2.85	0.139	0.446
15.25	107.2	4.37	0.156	0.649
12.00	82.3	6.03	0.191	1.040
		High-performance vehicle		
18.00	129.2	0.00	0.194	0.052
16.75	119.1	0.55	0.197	0.060
15.50	109.2	1.11	0.201	0.071
14.25	99.5	1.68	0.205	0.084
13.0	89.9	2.27	0.212	0.102

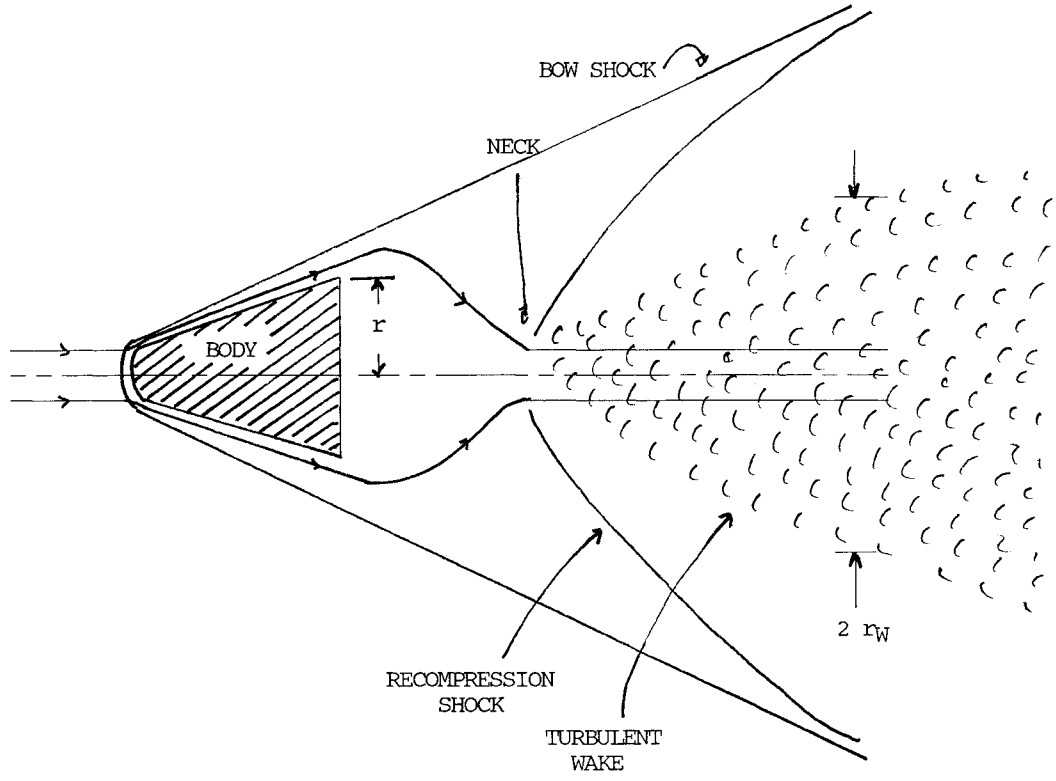

Fig. 3 Various important regions in an *RV* wake.

possible to comment briefly on its expected effects. In this region of the spectrum, the RV wake radiation is dominated by emissions from the neck and the turbulent region downstream of the neck. See Fig. 3. The radius of the neck region is approximately 60–75% of the base radius.[25] The radius of the outer boundary of the turbulent wake downstream of the neck is related[26] to the distance downstream from the RV by

$$r_w = 0.9r(C_D x_w)^{1/3}(2r)^{-1/3} \tag{45}$$

If viscous effects are neglected, C_D for sphere cones is given by

$$C_D = (r_N/r)^2 \cos^4\theta_c + 2\sin^2\theta_c \tag{46}$$

In general, the decay of wake intensity with axial distance is dependent upon many parameters. However, some general statements can be made by extrapolating from ballistic range measurements made at optical wavelengths and flow conditions roughly comparable with those considered here. According to Ref. 27, for a vehicle with a silica phenolic heat shield, the wake intensity decays exponentially with increasing values of x_w. At an axial distance equal to four times the base radius, the wake intensity per axial length has decayed to about 3% of the peak value from the body. At an axial location equal to 150 base radii, the wake intensity per axial length has further decayed to 0.1% of the peak body value. Using Eq. (45), the wake radius at this latter location for a vehicle with a base radius of 20 cm, a nose radius of 5 cm, and a cone angle of 7.5 deg is equal to 172% of the base radius. For this example, the wake radius varies linearly with base radius (with a deviation from linearity of less than 2%) for small changes in base radius. Since the contribution of the wake to the total vehicle radiation is small, the wake radius does not greatly exceed the base radius until the wake emissions have decayed substantially, and the wake radius varies linearly with base radius, the effects of the wake are not likely to change the earlier results.

Summary

A plausible aircraft mounted intensity interferometer should be capable of measuring the base radius of a nominal 20 cm base radius, 14,000 kg/m^2 ballistic coefficient re-entry vehicle (RV) to an uncertainty of 0.21 cm at a range of 277.5 km as long as the aircraft carrying the interferometer remains above the tropopause. The corresponding expected base radius uncertainty for measurements on a nominal 35 cm base radius, 8500 kg/m^2 ballistic coefficient RV is 0.55 cm. The tropopause lies at an altitude below the normal cruising altitude of transport aircraft, 10.67 km, at latitudes far from the equator in the winter. These accuracy figures include the degrading effects of photon shot noise, the attenuation of the optical emissions by the atmospheric absorption, the degrading effects of the turbulence in the aircraft boundary layer and the remainder of the atmosphere between the aircraft and the RV, and the uncertainty in the knowledge of the atmospheric structure constant. However, they do not include the effects of RV wake, which are beyond the scope of this present paper. Wake effects are not likely to modify these figures significantly, since the wake dimensions scale linearly with vehicle base radius for small changes in base radius.

Acknowledgments

The author would like to thank Andy Anderson, David Lush, Michael Kuchinos, and John Morris for their helpful discussions.

References

[1]Hanbury Brown, R. and Twiss, R. Q., "A New Type of Interferometer for Use in Radio Astronomy," *Philosophical Magazine,* Vol., 45, July 1954, pp. 663–682.

[2]Hanbury Brown, R. and Twiss, R. Q., "Interferometry of the Intensity Fluctuations in Light, I. Basic Theory: The Correlation Between Photons in Coherent Beams of Radiation," *Proceedings of the Royal Society of London,* Ser. A. Vol. 242, Royal Society of London, Nov. 1957, pp. 300–324.

[3]Hanbury Brown, R. and Twiss, R. Q., "Interferometry of the Intensity Fluctuations in Light, II. An Experimental Test of the Theory for Partially Coherent Light," *Proceedings of the Royal Society of London,* Ser. A, Vol. 243, Royal Society of London, Jan. 1958, pp. 291–319.

[4]Hanbury Brown, R. and Twiss, R. Q., "Interferometry of the Intensity Fluctuations in Light, III. Applications to Astronomy,"

Proceedings of the Royal Society of London, Ser. A. Vol. 248, Royal Society of London, Nov. 1958, pp. 199–221.

[5]Hanbury Brown, R. and Twiss, R. Q., "Interferometry of the Intensity Fluctuations in Light, IV. A Test of an Intensity Interferometer on Sirius A," *Proceedings of the Royal Society of London,* Ser. A, Vol. 248, Nov. 1958, pp. 222–237.

[6]Franon, M., *Optical Interferometry,* Academic, New York, 1966, pp. 181–189.

[7]Mensa, D. L., *High Resolution Radar Imaging,* Artech House, Dedham, MA, 1981.

[8]Feynman, R. P., Leighton, R. B., and Sands, M., *The Feynman Lectures on Physics,* Vol. III, Addison Wesley, Reading, MA, 1966, pp. 4-1–4-15.

[9]Friberg, A. T., "Effects of Coherence in Radiometry," *Optical Engineering,* Vol. 21, Sept.–Oct. 1982, pp. 927–936.

[10]Hufnagel, R. E. and Stanley, N. R., "Modulation Transfer Function Associated with Image Transmission through Turbulent Media," *Journal of the Optical Society of America,* Vol. 54, Jan. 1964, pp. 52–61.

[11]Hodara, H., "Effects of Turbulent Atmosphere on Phase and Frequency of Optical Waves," *Phase and Frequency Instabilities in Electromagnetic Wave Propagation,* AGARD CP-33, July 1976, pp. 673–688.

[12]Fried, D. L., "Optical Strength of Atmospheric Turbulence, Its Measurement and Its Effects on Optical Heterodyne Reception," *Phase and Frequency Instabilities in Electromagnetic Wave Propagation,* AGARD CP-33, July 1976, pp. 689-701.

[13]Bramely, E. N., "Some Aspects of the Rapid Directional Fluctuations of Short Radio Waves Reflected at the Ionosphere," *Proceedings of the Institution of Electrical Engineers,* Pt. B, Vol. 102, Institution of Electrical Engineers, London, July 1955, pp. 533–540.

[14]Gardiner, C. W., *Handbook of Stochasitic Methods for Physics, Chemistry and the Natural Sciences,* 2nd ed., Springer-Verlag, New York, 1985, pp. 57–59.

[15]Lorah, L. D. and Rubin, E., "Aerodynamic Influences of Infrared System Design," *Handbook of Military Infrared Technology,* U.S. Government Printing Office, Washington, DC, 1966, pp. 839–850.

[16]Streeter, J. J., "Boundary Layer Theory," *Handbook of Fluid Dynamics,* McGraw-Hill, New York, 1961, pp. 9–12.

[17]Sharma, A. B., Halme, S. J., and Butusov, M. M., *Optical Fiber Systems and Their Components,* Springer-Verlag, Berlin, 1981, p. 135–137.

[18]Bard, Y., *Nonlinear Parameter Estimation,* Academic, New York, 1974, p. 59.

[19]Martin, J. J., *Atmospheric Reentry,* Prentice-Hall, Englewood Cliffs, NJ, 1966, p. 37.

[20]Eden, R. C., "Heterojunction III-V Alloy Photodetectors for High-Sensitivity 1.06 μM Optical Receivers," *Proceedings of the IEEE,* Vol. 63, Institute of Electrical and Electronics Engineers, New York, Jan. 1975, pp. 32–37.

[21]*U.S. Standard Atmosphere Supplements, 1966,* U.S. Government Printing Office, Washington, DC, 1966, p. 107.

[22]Hufnagel, R. E., "Measurements of Atmospheric Turbulence via Observations of Instantaneous Optical Blur Functions," *Phase and Frequency Instabilities in Electromagnetic Wave Propagation,* AGARD CP-33, July 1976, pp. 703–709.

[23]Miller, M. G., Zieske, P. L., and Hanson, D., "Characterization of Atmospheric Turbulence," *Imaging through the Atmosphere,* Vol. 75, Society of Photo-Optical Instrumentation Engineers, Palos Verde, CA, March 1976, pp. 30–38.

[24]Miller, M. G. and Zieske, P. L., "Experimental Turbulence Profile and Parameters," *Optical Properties of the Atmosphere,* Vol. 142, Society of Photo-Optical Instrumentation Engineers, Palos Verde, CA, March 1978, pp. 98–103.

[25]Levenstein, Z. J. and Krumins, M. V., "Aerodynamics of Hypersonic Wakes," *AIAA Journal,* Vol. 5, Sept. 1967, pp. 1596–1602.

[26]Levenstein, Z. J., "Hypersonic Wake Characteristics behind Spheres and Cones," *AIAA Journal,* Vol. 1, Dec. 1963, p. 2848–2850.

[27]Weinberg, N., "Experimental Optical Radiation Data in the Wake Flow Fields of Ablating Reentry Vehicles," M.S. Thesis, Univ. of Tennessee, Knoxville, TN, Dec. 1977.

Notice to Subscribers

We apologize that this issue was mailed to you late. As you may know, AIAA recently relocated its headquarters staff from New York, N.Y. to Washington, D.C., and this has caused some unavoidable disruption of staff operations. We will be able to make up some of the lost time each month and should be back to our normal schedule, with larger issues, in just a few months. In the meanwhile, we appreciate your patience.